FUDMA Journal of Sciences (FJS)
ISSN online: 2616-1370
ISSN print: 2645 - 2944
Vol. 5 No. 4, December, 2021, pp 308 - 325
DOI: https://doi.org/10.33003/fjs-2021-0504-835

APPLICATION OF LANDSAT-8 OPERATIONAL LAND IMAGER AND SHUTTLE RADAR TOPOGRAPHY MISSION-DIGITAL ELEVATION MODEL IN THE STUDY OF IKARA AND ITS ENVIRONS, NORTHWESTERN NIGERIA

Abdulmalik, N. F[1]., Garba, I[2]., Abubakar, I. Y[2]., Muhyideen, H[2]., Agunleti, Y. S[2]., Magaji, S. S[2]., Aliyu, A. E.[2] and Umaru, A. O.[3]

[1]Centre for Energy Research and Training, Ahmadu Bello University, Zaria
[2]Department of Geology, Ahmadu Bello University, Zaria
[3]Department of Geology, University of Maiduguri
Corresponding Author's E-mail:- nanafatima88@gmail.com Tel:- +2348063380777

ABSTRACT
Images of the earth's surface captured by radiometric detectors on air-borne (satellite) sensors were employed in geologic reconnaissance survey. They were used to study rock units, pattern and trends of geologic structures on the surface in 2D. Multispectral resolution Landsat-8 Operational Land Imager (Landsat-8 OLI), have nine spectral band with spatial resolution of 30 m (bands 1 to 7, and 9) and 15 m for band 8. The aim of this research is to discriminate lithological units/complexes and delineate fractures (lineaments), hence, only bands 2 to 7 were used for this study. This technique was used to discriminate existing lithological units and identify major and minor extensive geologic structures within the study area. These selected bands were selected, grouped and combined (Band Combination (BC)) and processed for interpretation using applicable Software Packages. Hence, for each procedure and maximum clarity in the output of results, three bands were combined for each analytical process. Bands 4,3,2; 6,5,4; 7,5,3 were combined for Natural Colour Composite (NCC), False Colour Composite (FCC) and Principle Component Analysis (PCA) respectively. The results revealed two distinct lithological Complexes due to their similarities in appearance and differences in mineralogical compositions. SRTM-DEM was used to highlight the topography showing the lowest relief at the northeast and the highest relief at the south east. More so, elongated ridges of intermediate-high reliefs were exposed at the southern part of the study area trending NW-SE. A lineament map and Rose plot shows dominant trend of fractures to be NNW-SSE, NW-SE, N-S, NNE-SSW and NE-SW.

Key words: Band Composites, Landsat-8 OLI, Lineaments, Principal Component Analysis, SRTM-DEM,

INTRODUCTION

For efficiently mapping lithological units and generating lineaments at different scales, multispectral sensors such as Terra ASTER, Landsat 5 TM, Landsat 7 ETM+, Landsat 8 OLI, and Sentinel 2A are employed; also hyperspectral imagery data from hyperspectral satellite and airborne sensors such as EO-1 Hyperion and AVIRIS are used for lithological and mineralogical mapping due to their high spectral resolution in detecting hydrothermal alteration zones (Kruse *et al.*, 2003; Pour and Hashim, 2012; Pournamdari *et al*., 2014; Jellouli *et al*., 2019; Adiri *et al*., 2019). It creates an easy way to identify geologic structures, thus enabling better extraction of interpretable geologic features (Jakob *et al*., 2015). Landsat 8 Operational Land Imager (OLI) and Thermal Infrared Sensor (TIRS) images consist of nine spectral bands with wavelengths between 0.43 to 1.38 micrometres and spatial resolution of 30 meters for Bands 1 to 7 and 9. New band 1 (ultra-blue) is useful for coastal and aerosol studies. New band 9 is useful for cirrus cloud detection. The resolution for Band 8 (panchromatic) is 15 meters. The Landsat 8 satellite was launch on February 11, 2013 and carries both sensors, the Operational Land Imager (OLI) and Thermal Infrared Sensor (TIRS), these sensors covers the Visible and Near Infrared (VNIR), Short Wave Infrared (SWIR) and Thermal Infrared range (TIR) of the electromagnetic spectrum on 11 bands, including a deep blue coastal/aerosol band and a short-wave cirrus band. Operational Land Imager (OLI) multispectral sensor collect data in a range of spectral regions through the visible and near infrared (VNIR), short wave infrared (SWIR). OLI has 9 spectral bands, including 5 VNIR between 0.43 and 0.88 µm including coastal aerosol band, 3 SWIR bands between 1.57 and 2.29 µm including the Cirrus band (Tables 1 and 2). We used the OLI level-1T (Corrected Terrain) data product from the Land Processes Distributed Active Archive Center at NASA. The Landsat 8 OLI image is radiometrically calibrated, geometrically co-registered and orthorectified. Landsat 8 OLI image scene are characterized by a high radiometric resolution (16 bits), and the scenes cover 185 x 180 km, available at free of charge.

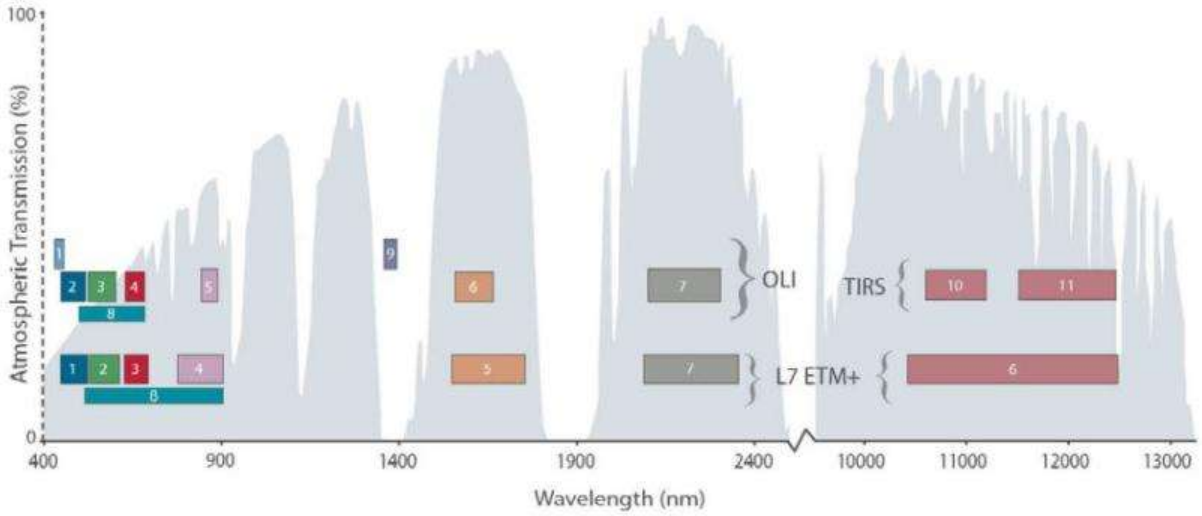

Fig. 1: Bandpass wavelength (spectral resolution) comparisons between Landsat-8 (OLI) and Landsat-7 (ETM+) (USGS, 2013).

Table. 1: Landsat-8 OLI bands with spectral and spatial resolutions (USGS, 2013)

Bands	**Wavelength (micrometers)**	**Resolution (meters)**
Band 1 - Coastal aerosol	0.43-0.45	30
Band 2 - Blue	0.45-0.51	30
Band 3 - Green	0.53-0.59	30
Band 4 - Red	0.64-0.67	30
Band 5 - Near Infrared (NIR)	0.85-0.88	30
Band 6 - SWIR 1	1.57-1.65	30
Band 7 - SWIR 2	2.11-2.29	30
Band 8 - Panchromatic	0.50-0.68	15
Band 9 - Cirrus	1.36-1.38	30

Table. 2: Landsat-7 ETM+ and Landsat-8 OLI and TIRS spectral resolution and bands comparison (GIS Stack Exchange, 2021)

Landsat-7 ETM+ Bands (μm)			Landsat-8 OLI and *TIRS* Bands (μm)		
			30 m Coastal/Aerosol	0.435 - 0.451	Band 1
Band 1	30 m Blue	0.441 - 0.514	30 m Blue	0.452 - 0.512	Band 2
Band 2	30 m Green	0.519 - 0.601	30 m Green	0.533 - 0.590	Band 3
Band 3	30 m Red	0.631 - 0.692	30 m Red	0.636 - 0.673	Band 4
Band 4	30 m NIR	0.772 - 0.898	30 m NIR	0.851 - 0.879	Band 5
Band 5	30 m SWIR-1	1.547 - 1.749	30 m SWIR-1	1.566 - 1.651	Band 6
Band 6	60 m TIR	10.31 - 12.36	*100 m TIR-1*	*10.60 – 11.19*	Band 10
			100 m TIR-2	*11.50 – 12.51*	Band 11
Band 7	30 m SWIR-2	2.064 - 2.345	30 m SWIR-2	2.107 - 2.294	Band 7
Band 8	15 m Pan	0.515 - 0.896	15 m Pan	0.503 - 0.676	Band 8
			30 m Cirrus	1.363 - 1.384	Band 9

GEOLOGY OF THE BASEMENT COMPLEX

The Nigerian Basement Complex evolved as a result of the collision of the West African Craton, Congo Craton and the East Saharan block (Black *et al*., 1994). The West African Craton subducted beneath the Congo Craton (Ball, 1980; Wright *et al*., 1985). It is considered as the southern prolongation of the Central Hoggar (McCurry, 1976) and sometimes called Neoproterozoic Trans-Saharan Belt. Caby (1989) and Boullier (1991) suggested that the Neoproterozoic Trans-Saharan Belt stretches from North Africa to Brazil, formed by multiple collisions of island arcs, sedimentary basins and continental fragments dating as far back as 750-500Ma (Wright *et al.*, 1985; Ajibade and Wright, 1989). It consists of older crust of Archean and Palaeo-proterozoic ages (Grant, 1970; Grant *et al*., 1972; Oversby, 1975). This gave rise to several deformational features, metamorphism and extrusion of alkaline to calc-alkaline volcanics (McCurry and Wright, 1977; Holt *et al*., 1978). This also led to the reactivation of the belt where the Nigerian Basement Complex lies (Turner, 1983; Fitches *et al*., 1985; Wright *et al*., 1985); which is to the east of West African Craton, northwest of Congo Craton and to south of the Taureg shield by Burke and Dewey (1972); Black *et al*. (1979); LeBlanc (1981) and Caby *et a*l. (1981). The reactivation that affected the whole region was during the Pan-African Orogeny (600±150ma). The Nigerian basement is made up of the Tertiary to Recent sediments; Tertiary volcanics; Cretaceous sediments; Jurassic Younger Granites and the Precambrian basement rocks (Obaje, 2009). In other words, the major litho-stratigraphical units in the Nigerian Basement Complex are: Migmatite-Gneisses, Schist Belts, the Older and Younger Granite Complexes. It covers major parts of the north, northwest, southwest and parts of north-central, eastern and southern regions. However, about 50% of the Nigerian Basement Complex is covered by sediments of Cretaceous to Recent age (Woakes *et al.*, 1987) (Fig. 2).

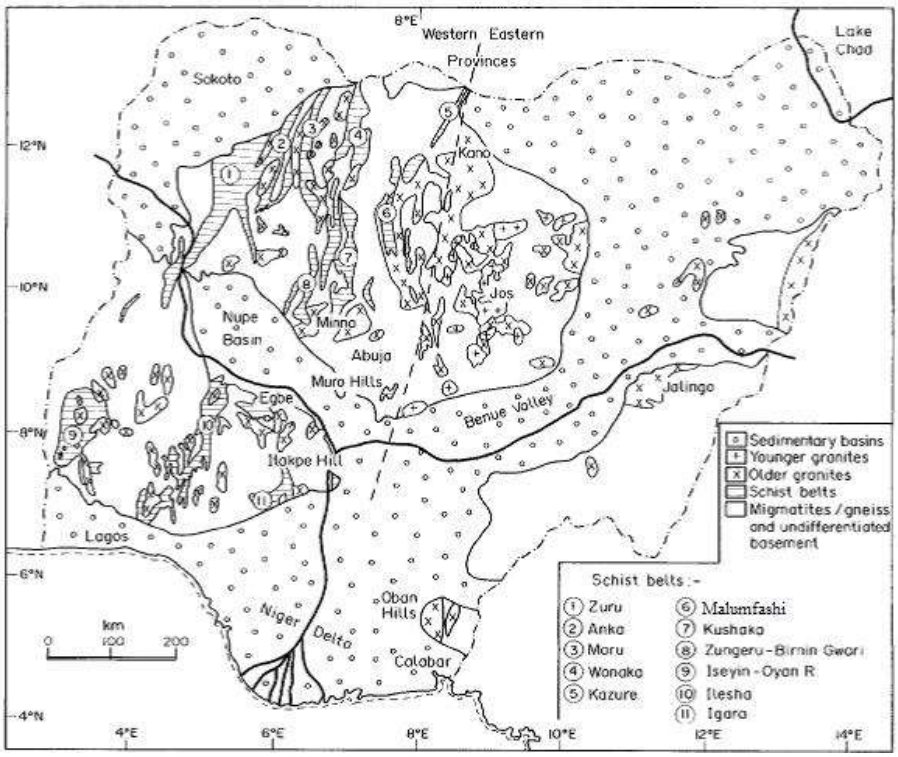

Fig. 2: Geological map of Nigeria showing the Precambrian Basement Complex, Schist Belts and Sedimentary Basins (Woakes *et al.*, 1987).

LOCATION OF STUDY AREA

The study area selected for the research is situated at the northwestern part of Nigeria, Kaduna State. It is bounded by Latitudes 11° 00' 00" N to 11° 30' 00" N and by Longitudes 08° 00' 00" E to 08° 30' 00" E (Fig. 3). It is on a scale of 1:100,000 and about 3,031.7 square kilometers. It has several rivers and forest reserves. It is underlain by migmatites, gneisses and granitic rocks. Places were accessed via minor and major roads, foot paths, river channels and cattle tracks.

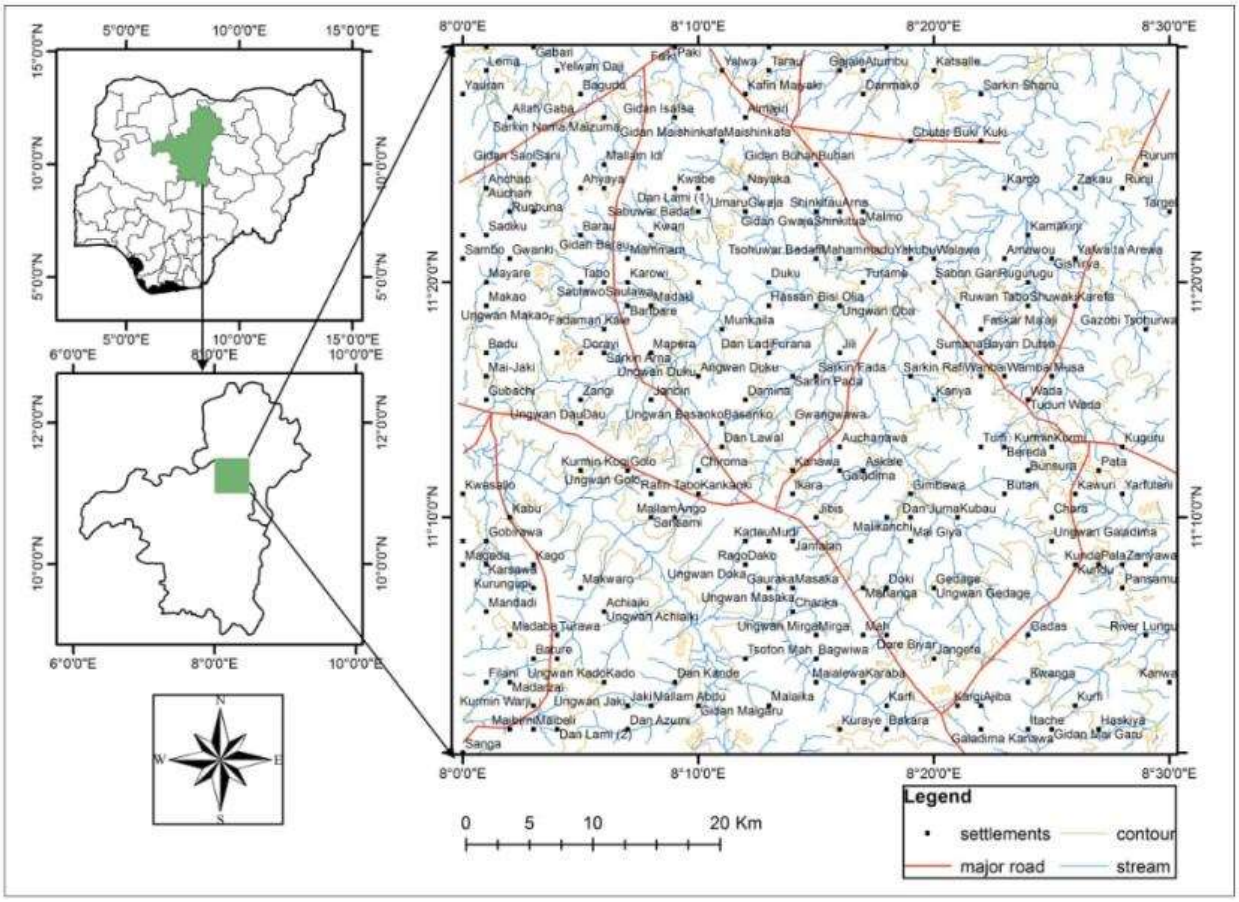

Fig. 2: Map of study area.

MATERIALS AND METHODS

Interested satellite imagery bands of Landsat-8 Operational Land Imager (OLI) 2, 3,4,5,6 and 7 were downloaded from Earth Explorer data base (**https://earthexplorer.usgs.gov/**). These are bands from the visible light (bands 2, 3 and 4), near infrared (band 5) and shortwave infrared I and II (bands 6 and 7) of the electromagnetic spectrum. However, one can equally choose to download these satellite images/bands via Global Mapper Software. Band combinations (Natural and False Colour Combination; and Principal Component Analysis) were produced and used in discriminating existing rock types, identification of geologic structures and drainage pattern of the area. The software used for the band combinations is ENVI Software. The sensor used in the acquisition is the Landsat-8 OLI; acquired on the *2nd of February*, 2021; at a processing collection level of *L2SP;* Paths and Rows from which the study was carved out from are *188-052* and *189*-052, this was because the study area is between two scenes of the Landsat series; Collection and Real Time (Tier) at 2 and 1 respectively (*C2:T1*). Below are the properties of the satellite images in summary:

LC08_L2SP_188052_20210202_20210303_02_T1
LC08_L2SP_189052_20210209_20210302_02_T1

The scenes were mosaicked using ArcGIS Software for pre-processing before the coordinates of the study area was extracted to form a composite map. The spectral and spatial resolution properties of the bands to be used has already been discussed and tabled above. NCC, FCC and PCA involve the linear combination of selected bands used to discriminate lithological units and define geological structures exposed on the surface of the study area. This will aid in updating the geological map of the study area. This methodology employed for the satellite image analysis for lithological discrimination and structural features is similar to the works of Acharya and Yang (2013); USGS (2013), Mwaniki *et al.* (2015), Amusuk *et al.* (2016) and Abdelaziz *et al.* (2018).

The scenes were the study area lies had to be mosaicked because it falls on two different paths, then the bands of interest will be acquired. Before the Band Combinations, the Landsat-8 bands were selected, layer stacked and then rearranged accordingly in the software. The bands used for each colour combination process is highlighted; the first band is placed on the "R", the second on "G" and the third on "B", it gets loaded and saved. These images were then exported (as they are already georeferenced) using Global Mapper software to have the exact coordinates of the study area. For the Principal Component Analysis, the same format of false image composite was followed but principal component was selected followed by a forward principal component rotation to compute new statistics, hence, spatial subsets for the bands was selected before loading RGB. Using this was to further boost the areas where certain rock types are and buttress the definite presence and results of major fractures/faults in the area.

For the principal component analysis, the same format of false image composite was followed but principal component was selected followed by a forward principal component rotation to compute new statistics, hence, spatial subsets for the bands was selected before loading RGB. The bands selected were 7, 5 and 3; this combination has less noise. Using this was to further boost the areas where certain rock types are and buttress the definite presence and results of major fractures/faults in the area. The Digital Elevation Model (DEM) was produced using Global Mapper Software were by the satellite data was acquired from Shuttle Radar Topographic Mission (SRTM-DEM). This data was acquired and enhanced to give a clear distinction between the topographic levels and the lineament features within the study area. This was carried out by searching in the Global Land Cover Facility; search for the map area by inserting the latitude and longitude coordinates and SRTM (Shuttle Radar Topographic Mission) was selected and then downloaded. It was then saved and used for the intended analysis. This model was then transferred to Global Mapper to extract the bounds of the study area. The colour ramp shader was used to give the varying elevations (slopes) from high to medium to low; shaded relief images were created by varying the angle of the sun of the DEM using Global Mapper software.

RESULTS AND DISCUSSION

Bands 4,3,2 was combined for natural colour composite and 6,5,4; 7,6,4 and 7,5,3 for false colour composites. As observed from the natural colour composite (NCC) image in Fig. 4, there appears to be a sharp contrast between rock units by a geologic feature (fracture), possibly a fracture trending NW-SE. These rock units are displayed in reddish-white, greyish-white and faint brown contrasts. The spots in black, light turquoise and seaweed green are water. The differences in coloration could be as a result of water plants/weeds, silts or sediments of different rock types washed into them. As observed from the false colour composite (FCC) images in Figs. 5, 6 and 7 unlike the NCC, there seem to be almost no differentiation amongst the rock units. This could be as a result of similarities in the mineralogical components of the rocks. These results were generated from Shortwave Infrared I and II, Near Infrared, Green and Red bands combined in three separate modes (as written above). From the works of Acharya and Yang (2013) and USGS (2013), their results after carrying out band composites of Red (4), Green (3) and Blue (2) for natural colour combination; and Shortwave Infrared I (6), Near Infrared (5) and Red (4) for false colour combination respectively, showed wetlands from drylands; and rock units that looked similar. And from the current study area, the results show similar rock units observed in Figs. 4 and 5. From the works of Mwaniki *et al.* (2015), Shortwave Infrared bands I and II (6 and 7) with a band of the visible light (Red-4) was combined to display several lithological components. However, in Fig. 6, the study area is covered by lithological units that are similar, just like in Fig. 5. Amusuk *et al.* (2016) also carried out FCC by combining bands 7,5,3 to enhance rock exposures. Using this band combination for the current study area, the result was similar to Figs. 5 and 6 (Fig. 7). Also, Amusuk *et al.* (2016) carried out band ratio composite (BR) by combining bands of Shortwave Infrared I and II (6 and 7), Near Infrared (5), Blue and Red (2 and 4) of the visible light. These were combined in ratios of 7/5;6/5;2/4 to discriminate volcanic rocks from granitic rocks. However, this study area has no reports of the occurrences of volcanic rocks hence, the result shows rock units that are similar, possibly in mineralogical components (granitic, gneissic and migmatitic rocks) (Fig. 8). The mineralogical components of migmatites, gneisses and granites are quite similar, but the texture or tectonic fabrics are different, hence, lithological discrimination is limited. The areas/spots in black and blue (Northeastern part) are areas covered by water. However, since the FCC are all similar in appearance, Principle Component Analysis (PCA) with bands 7,5,3 was carried out (Fig. 9). This also shows similarities in lithologies; whereas the southwestern part is a valley-like feature with several river channels (greenish) drawn to it, trending NW-SE. A large water body at the northeast is displayed in blue also. The geological map of the study area as reported by the Nigerian Geological Survey Agency (2009), the rocks at the west, southwestern and south are mainly granitic rocks of the Older Granite Complex. While at the southeast, east, northeast, north and northwest, the dominant rocks are migmatites and gneisses of the Migmatite-Gneiss Complex. There are pockets of granitoid intrusions in the Migmatite-Gneiss Complex and some gneisses identified in areas with more of granitic rocks. However, the migmatites and gneisses are older than the granitic rocks.

These are fault zones with shear zones identified especially along the NW-SE fracture zones. Both cataclastic rocks and sheared rocks of granites, granodiorites, gneisses, migmatites, brecciated quartzites and mylonites were identified. However, most parts of the fracture/fault lines have been concealed while some are identified by aligned vegetation, discontinuous quartzite ridges, trenches or burrows, drainage patterns and structurally controlled water ways. Structural lineaments within the study area representing geological structures such as the fractures, were extracted and a Rose diagram was plotted which showed the major trends or orientations of the fractures in descending order to be towards NNW-SSE, NW-SE, N-S, NNE-SSW and NE-SW (Figs. 10 and 11). More so, drainage pattern identified to be most occurring are dendritic in nature. These drainages at the southwestern part of the study area has water flow towards its central point like a valley; while drainages identified at the central part of the study area has water flow towards the northeastern part of the study area being the lowest part where a dam is situated.

The Digital Elevation Model (Fig. 12), displays the lowest relief areas situated at the northeast where the dam and forest reserves are (from 550m and below); areas with moderate relief above sea level trends northwest-southeast by the conspicuous lithological demarcation (±650m). This is suggested to be an elongated ridge; and the areas with highest relief above sea level are situated at the southwestern and southeastern corners of the map (from 700m and above). However, the topographic data attained from DEM were classified. The essence of classifying the topographic data is to group areas within the same relief range and give a good clarity on the topographic differences

using designated colours representing low, moderate and high reliefs (Fig. 13). The elevations were made at an interval of 50 meters above sea level. Fig. 14 is the 3D view of the Digital Elevation Model displaying the elongated ridge earlier suggested in "Red", the highest points in "Purple" and the lowest parts in "Blue". The relief area in green flanked by areas in yellow/red in the southwest (Figs. 12, 13 and 14), is possibly a valley/trench trending NW-SE.

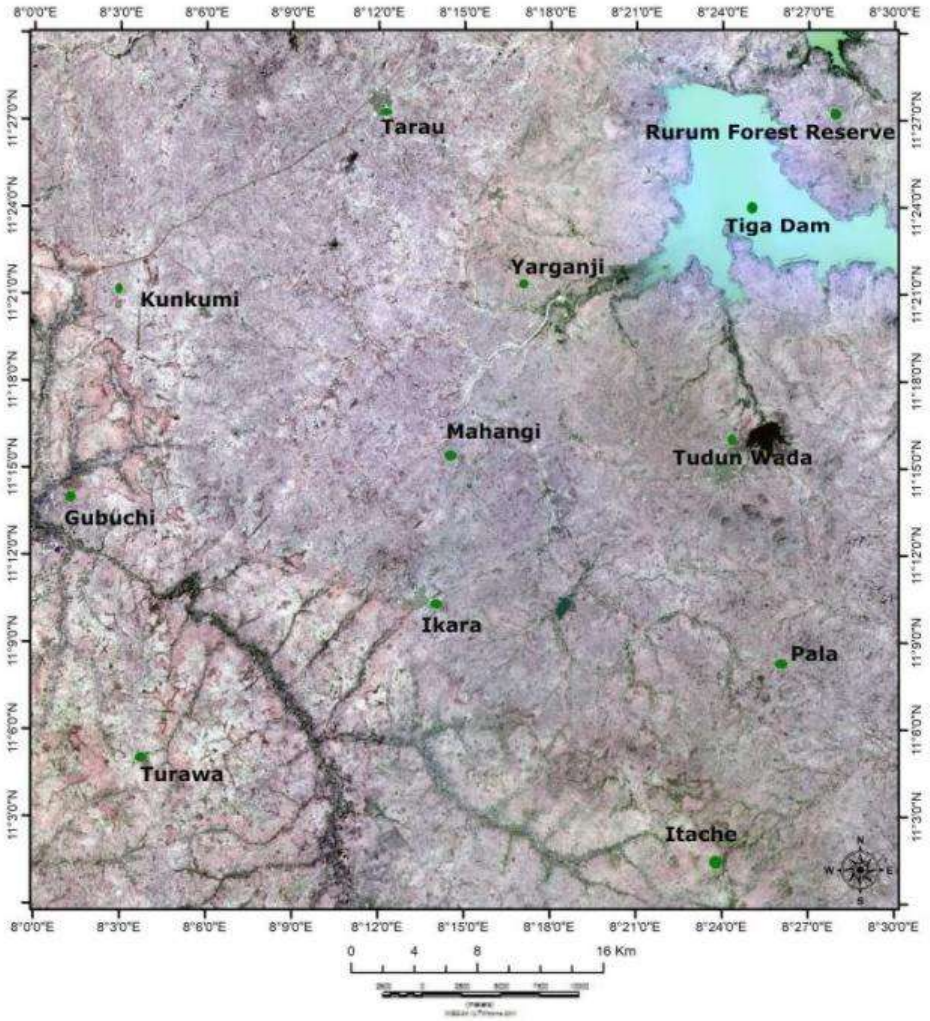

Fig. 4: Landsat image of study area displaying the natural colour composite of bands 4,3,2.

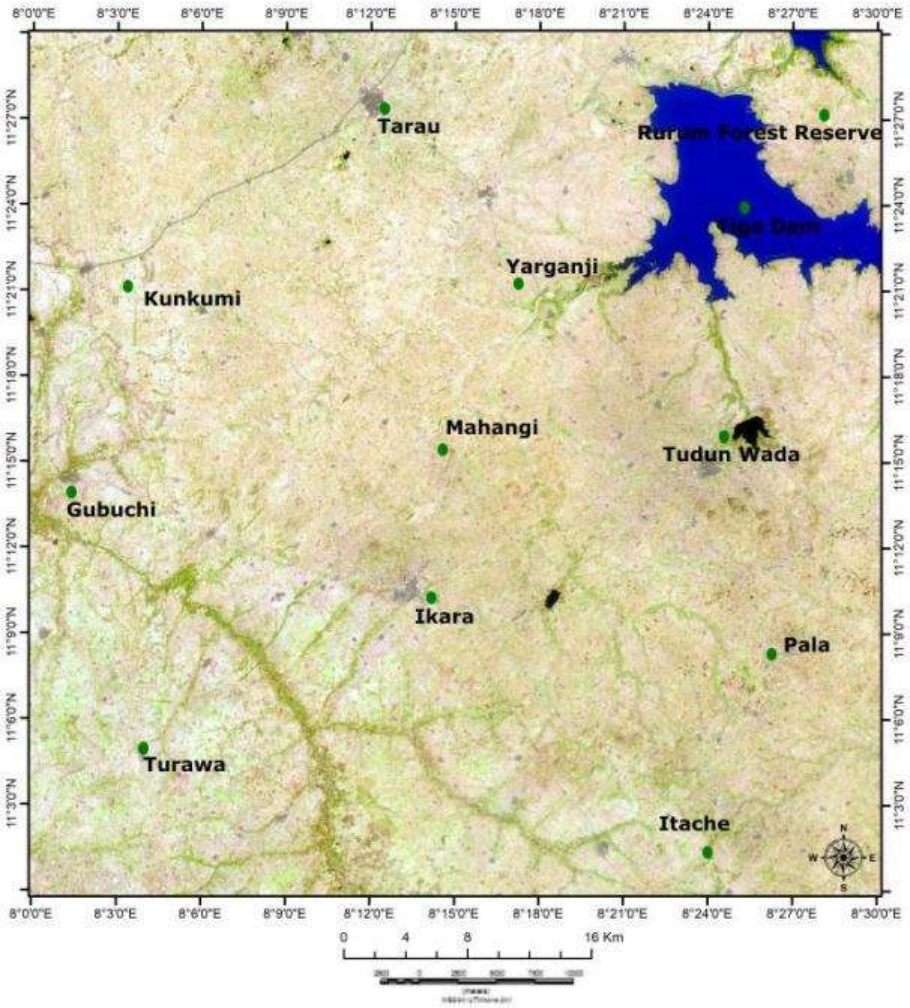

Fig. 5: Landsat image of study area displaying the combination result of bands 6,5,4 (FCC).

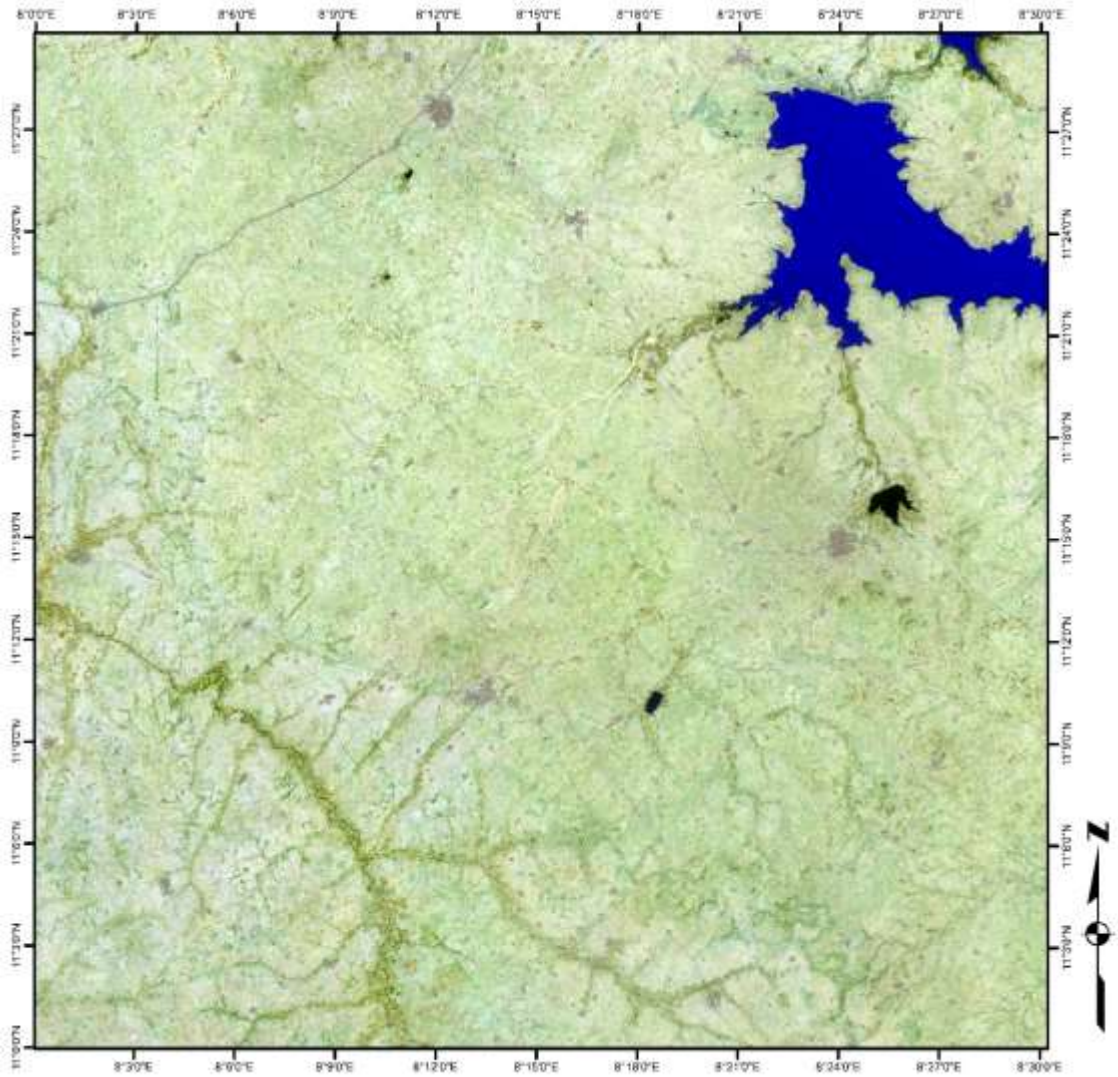

Fig. 6: Landsat image of study area displaying the combination result of bands 7,6,4 (FCC).

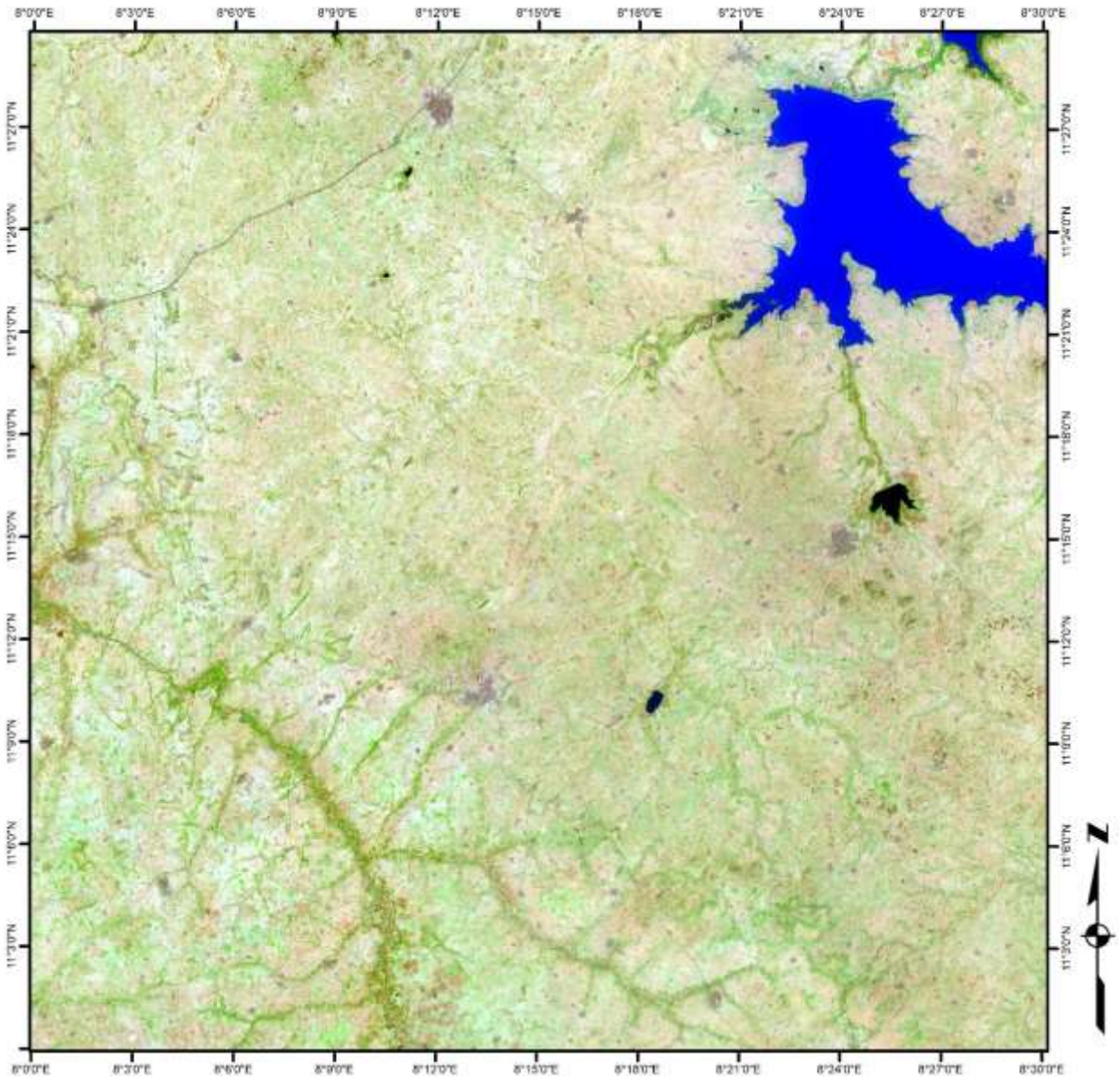

Fig. 7: Landsat image of study area displaying the combination result of bands 7,5,3 (FCC).

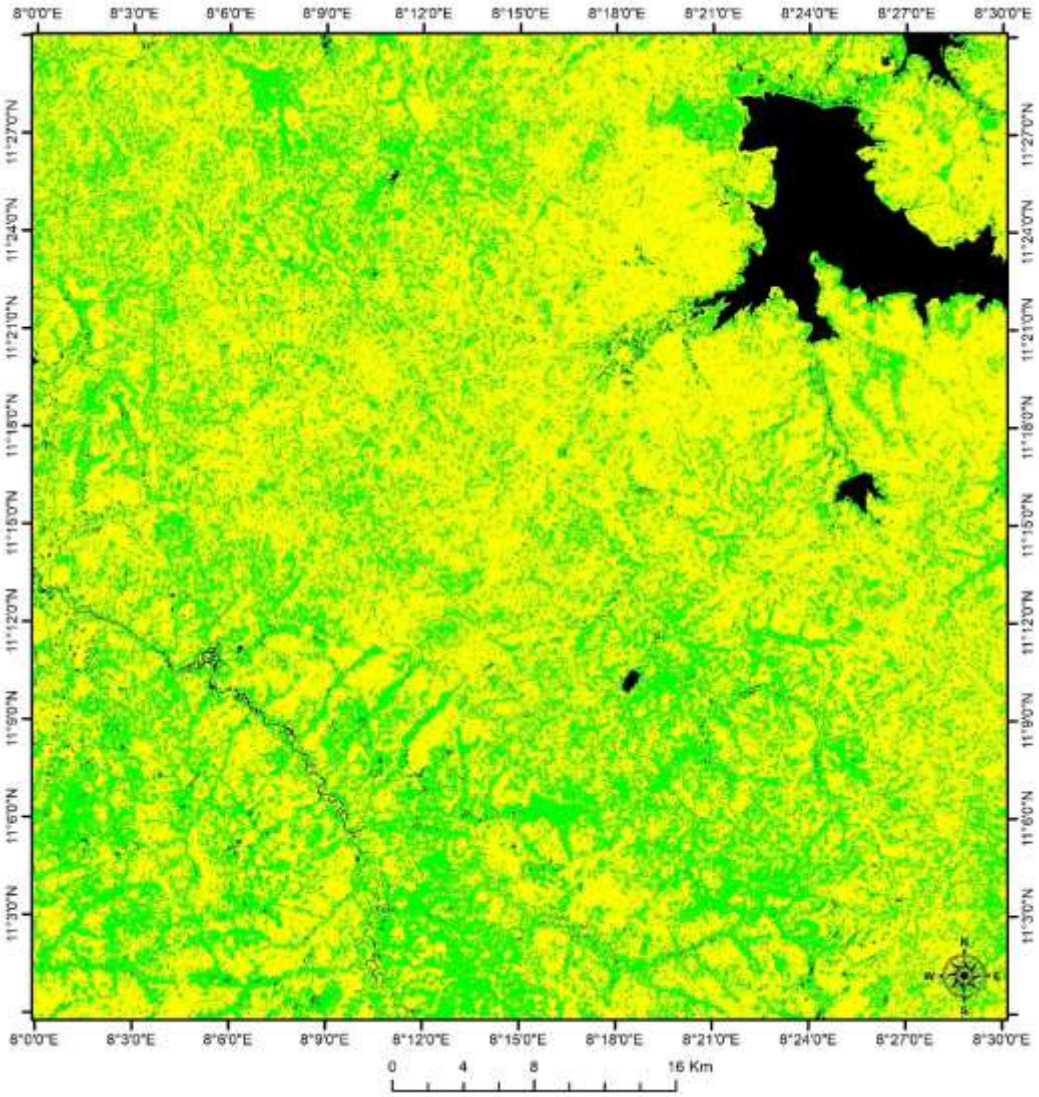

Fig. 8: Landsat image of study area displaying the combination result of bands 7/5;6/5;2/4 (FCC).

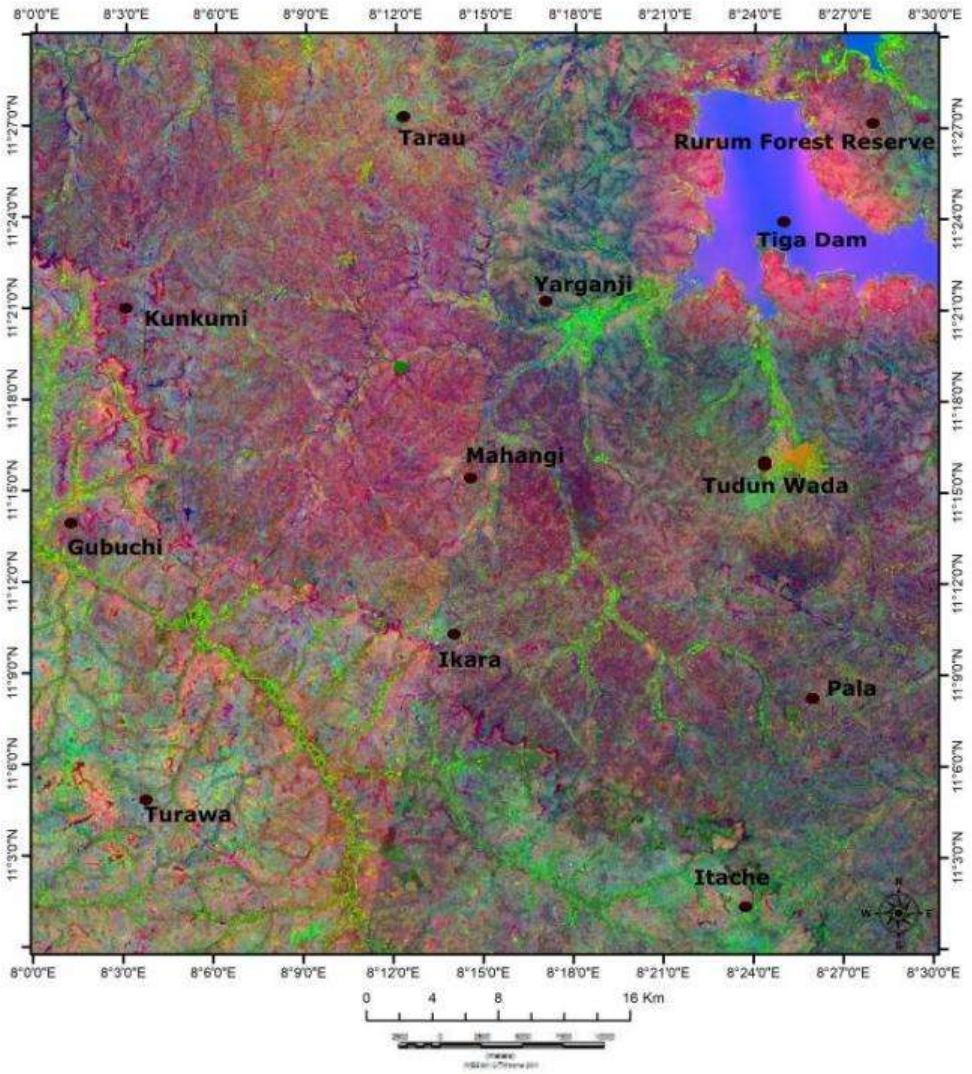

Fig. 9: Principal Component Analysis of study area (bands 7,5,3).

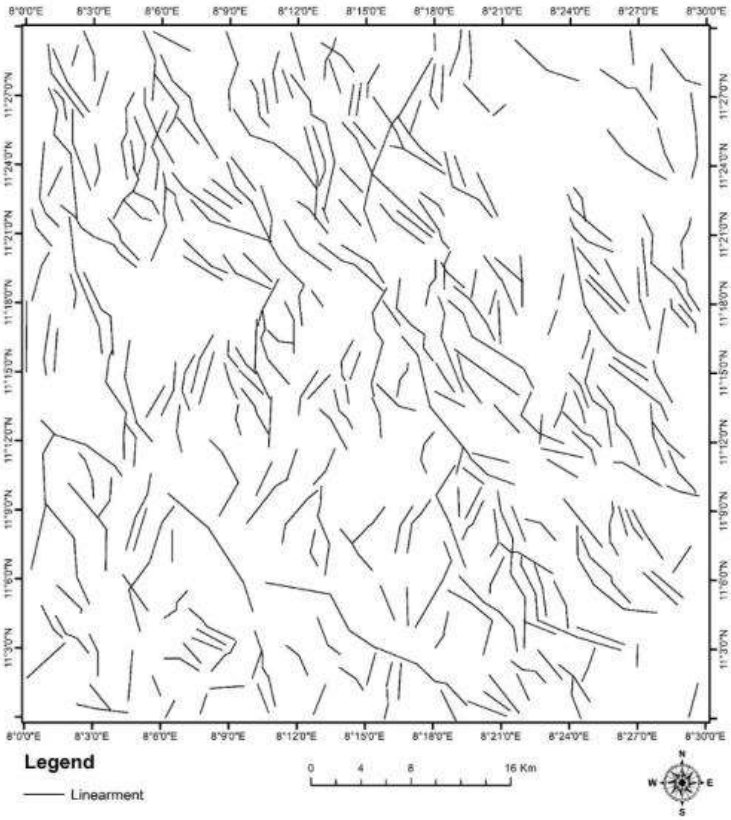

Fig. 10: Lineament map displaying the fractures been extracted from the FCC Landsat image of the study area.

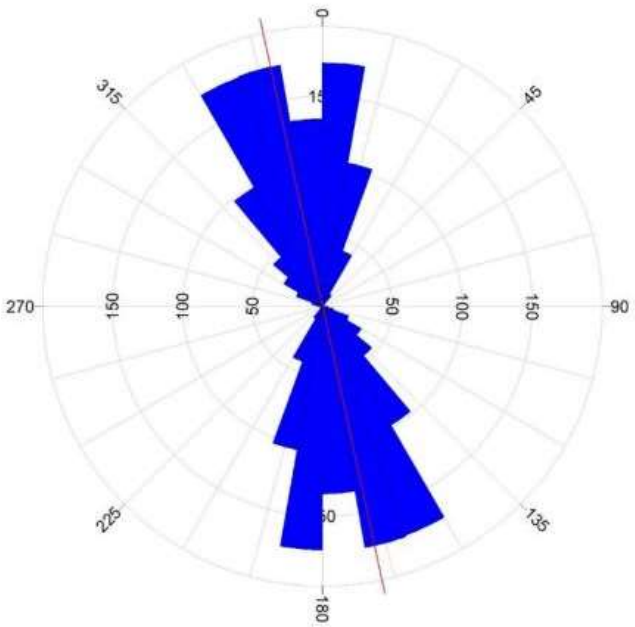

Fig. 11: Rose diagram showing the dominant trend direction of lineaments from the Landsat-8 as NW-SE.

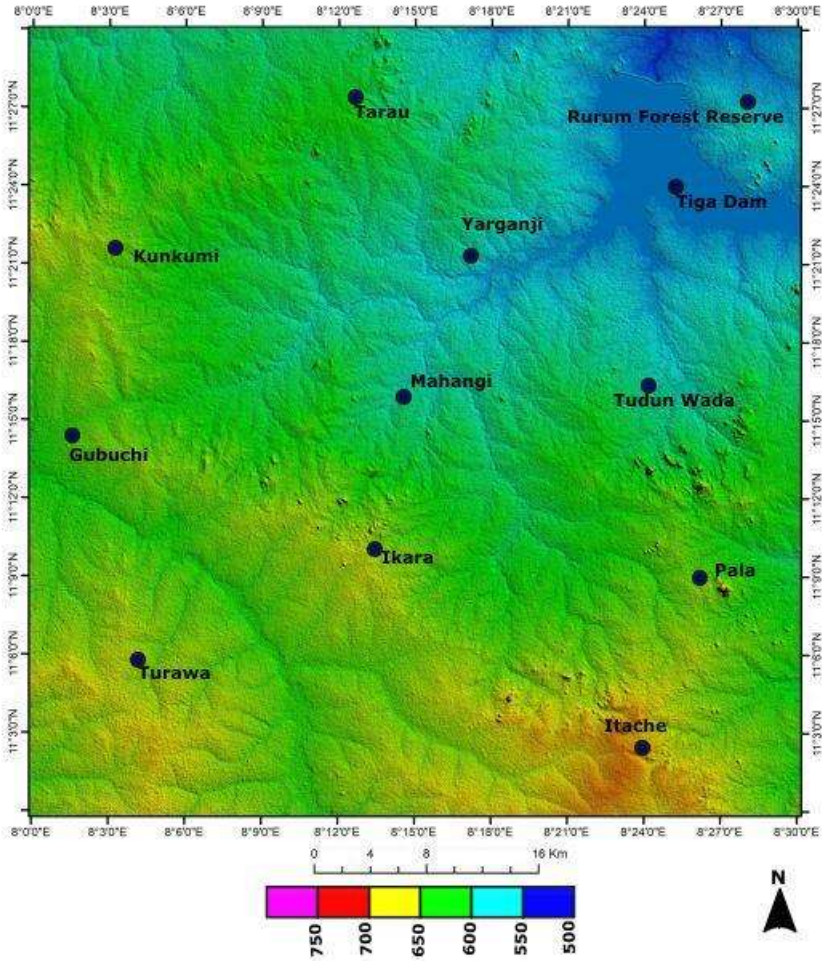

Fig. 12: Digital Elevation Model showing topographic differences across the study area.

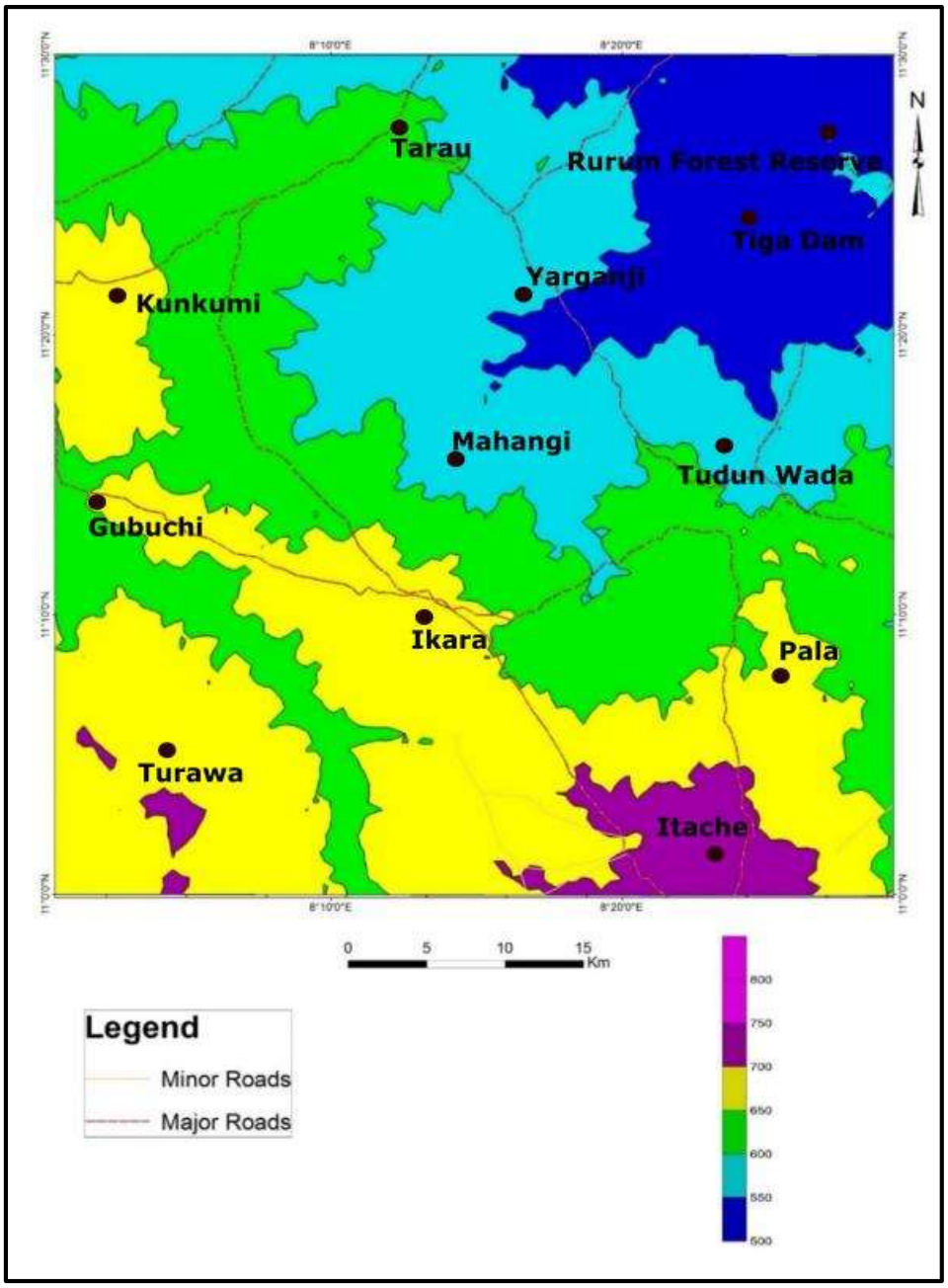

Fig. 13: Classified Digital Elevation Model showing topographic differences across the study area.

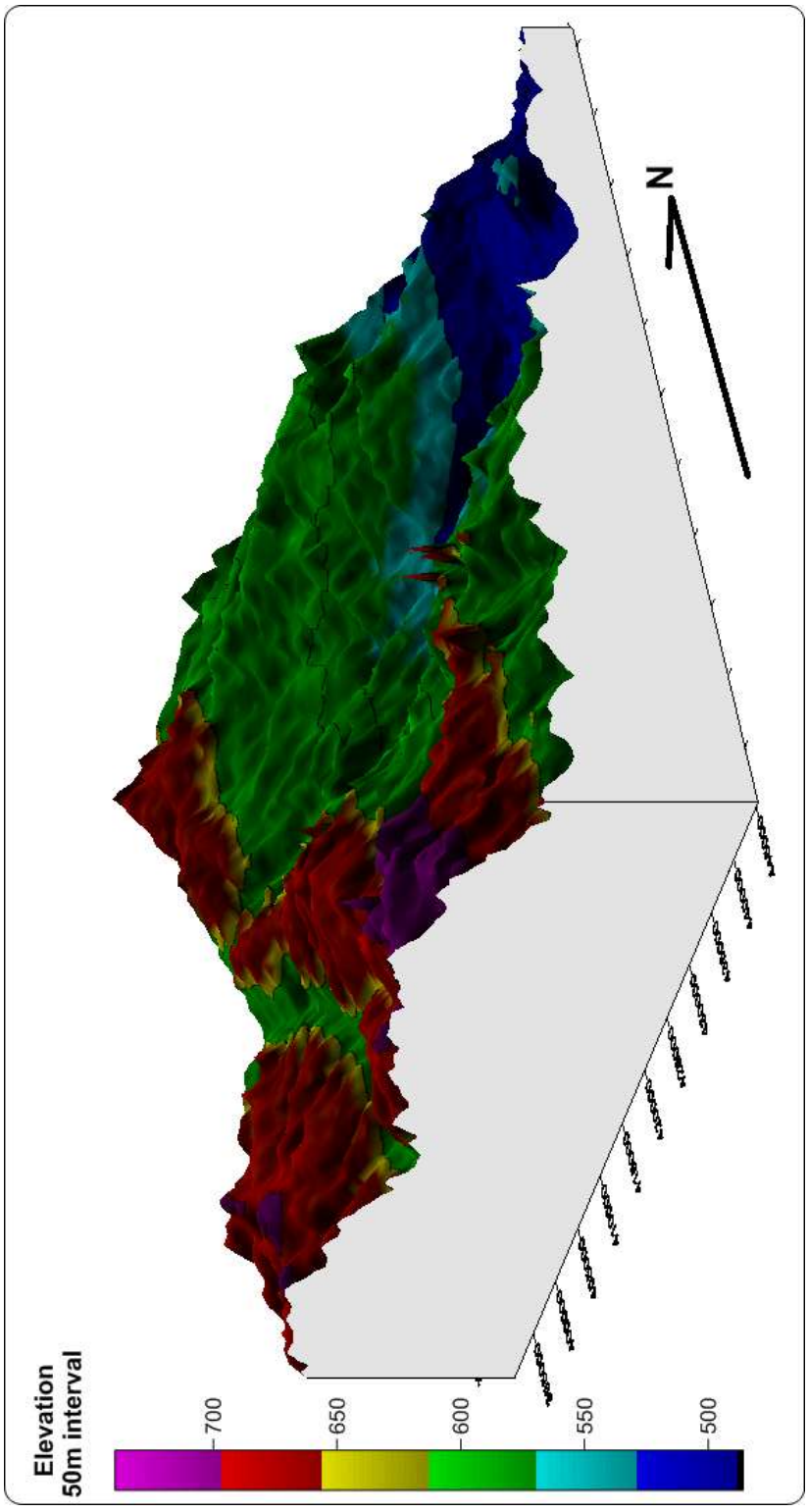

Fig. 14: 3D view of the Digital Elevation Model displaying the elongated ridges in "Red", the highest points in "Purple"and the lowest parts in "Blue".

CONCLUSION

The use of remote sensing has been efficient in solving earth science problems, particularly geologic problems. This has aided in solving lithological and structural mapping issues in relative shorter times thus, saving cost and time. Band combinations have proven to be quite useful in identifying rock units or at a regional scale, lithological complexes as the case may be. Rocks vary in fabric, texture and

mineralogical/chemical compositions, hence the colour contrasts exhibited after bands of geological importance have been merged, shows little lithological discrimination. As explained above, there are still intrusions or exposures of different petrology within the discriminated complexes. Major fracture/fault lines have been identified and are exhibited on field as extended trenches, aligned vegetation, discontinuous ridges, aligned rock exposures and drainage patterns. However, some are not exposed on the surface and some structurally control river channels. The fractures are oriented majorly towards the NW-SE direction as the maximum stress axis acted along the NE-SW direction. The fractures mainly identified are sinistral strike-slip faults with some zones of dip-slip faults (mostly normal faults). Shear zones were also significantly wide spread with conspicuous sheared rocks and shear zone indicators like mantled porphyroblasts, foliation curvature and marker displacements (sheared veins) exhibited on some lithological units. In addition, there are conjugate NE-SW fracture lines identified by the northeast and southeast, and a regional N-S fracture line also identified at the west of the study area. This shows that the study area was affected on a regional scale by a major fault trending NW-SE, complementary to the NW-SE wrench faults and N-S shear zones of Hoggar Aïr, southern Niger Republic.

ACKNOWLEDGEMENT

The authors appreciate the United State Geological Survey (USGS) for making the Landsat-8 Operational Land Imager (OLI) bands available through Earth Explorer, and the Global Land Cover Facility for making ESRI satellite data available for elevation models; they were all used strictly for research purposes.

REFERENCES

Abdelaziz, R., El Rahman, Y. A. and Wilhem, S. (2018). Landsat-8 data for chromite prospecting in the Logar Massif, Afghanistan.

Acharya, T. D and Yang, I. (2015). Exploring Landsat-8. International Journal of IT, Engineering and Applied Sciences Research (IJIEASR)., Vol. 4 (4), pp. 4-10.

Adiri, Z., El Harti, A., Jellouli, A., Maacha, L., Zouhair, M. and Bachaoui, E. M. (2019). "Mapping copper mineralization using EO-1 Hyperion data fusion with Landsat 8 OLI and Sentinel-2A in Moroccan AntiAtlas," Geocarto Int., vol. 0, no. 0, pp. 1–20.

Ajibade, A.C. and Wright, J.B. (1989). The Togo-Benin-Nigeria shield: evidence of crustal aggregation in Pan-African belt. *Tectonophysics*: **165**, pp. 125-129 and 433-449.

Amusuk, J. D., Hashim, M., Pour, A. B. and Musa, S. A. (2016). Utilization of landsat-8 data for lithological mapping of basement rocks of plateau state north central Nigeria. The International Archives of the Photogrammetry, Remote Sensing and Spatial Information Sciences, Volume XLII-4/W1. International Conference on Geomatic and Geospatial Technology (GGT) 2016, 3–5 October 2016, Kuala Lumpur, Malaysia.

Ball, E. (1980). An example of very consistent brittle deformation over a wide intracontinental area: The Late Pan-African fracture system of the Taureg and Nigerian shield. *Tectonophysics*: 16: 363-379.

Black, R., Ball, E., Bertrand, J.M.L., Boullier, A.M., Caby, R., Davison, I., Fabre, J., Leblanc, M. and Wright, L.I. (1979). Outline of the Pan-African geology of Adrar des Iforas (rep. of Mall). Geol. Rundsch. 68(2): 543-564.

Black, R., Latouche, L., Liegeois, J.P., Caby, R., Bertrand, J.M. (1994). Pan African displaced terranes in the Taureg shield (Central Sahara). Geology (22): 641-644.

Boullier, A.M. (1991). The Pan-African Tran-Saharan belt in the Hoggar shield (Algeria, Mali.Niger): a review. *In:* DALLMEYER, R.D. &LEC'ORC'HE, J.P. (editors) *The West African Orogens and Circum-AtlanticCorrelatives.* Springer-Verlag, Berlin, pp.85-105.

Burke, K.C. and Dewey, J.F. (1972). Orogeny in Africa; In: African Geology, edited by Dessauvagie, T.F.J. and Whiteman, A.J. University of Ibadan. Pp. 583-608.

Caby, R., Bertrand, J.M.L. and Black, R. (1981). Pan-African ocean closure and continental collision in the Hoggar-Iforas segment Central Sahara: In Precambrian Plate Tectonics. Kröner, A. (Editor); Elsevier Amsterdam, pp. 407-434.

Caby, R., (1989). Precambrian terranes of Benin- Nigeria and northeast Brazil and the late Proterozoic South Atlantic fit. Geological Society America Special Paper (**230**), pp. 145-158.

Fitches, R.W., Ajibade, A.C., Egbuniwe, I.G., Hole, R.W., Wright, J.B. (1985). Late Proterozoic Schist Belts and Plutonism in Northwestern Nigeria: *Journal of Geological Society London*, 142:319-337.

Geographic Information System Stack Exchange (gisstackexchange). (2021). *https://gis.stackexchange.com/questions/183758/difference-between-landsat-7-and-landsat-8-toa-reflectance-computation.*

Grant, N.K. (1970). Geochronology of Precambrian basement rocks from Ibadan, southwestern Nigeria. *Earth Planetary Science Letters*. 10: 29-38.

Grant, N.K., Hickman, M., Burkholder, F.R. and Powell, J.L. (1972). Kibaran metamorphic belt in the Pan-African domain of West Africa, nature (London), 134: 343-349.

Holt, R.W., Egbuniwe, I.G, Fitches, W.R. and Wright, J.B. (1978). The relationship between low grade metasedimentary belts, calc-alkaline volcanism and the Pan-African orogeny in northwestern Nigeria: *GeologischeRundschau.*, **67**, pp. 631-646.

Jakob, S., Buhler, B., Gloaguen, R., Breitkreuz, C., Eliwa, A. H., and El Gameel, K. (2015). Remote sensing based improvement of the geological map of the Neoproterozoic Ras Gharib segment in the Eastern Desert (NE–Egypt) using texture features. Journal of African Earth Sciences, Elsevier, vol. 111, pp. 138-147.

Jellouli, A., El Harti, A., Adiri, Z. , Bachaoui, E. M. and El Ghmari. A. (2019). Application of Remote Sensing Data in Lithological Discrimination of Kerdous Inlier in the Anti Atlas Belt of Morocco. INTERNATIONAL JOURNAL ON INFORMATICS VISUALIZATION; vol 3(2-2), pp. 227-232

Kruse, F. A., Boardman, J. W. and Huntington, J. F. (2003). "Comparison of Airborne Hyperspectral Data and EO-1 Hyperion for Mineral Mapping," vol. 41, no. 6, pp. 1388–1400.

Leblanc, M. (1981). The Late Proterozoic Ophiolites of BouAzzer (Morocco) evidence for Pan-African plate tectonics: In Precambrian Plate Tectonics. Kroner, A. (Editor): *Elsevier*, Amsterdam. P. 435-451.

McCurry, P. (1976). The Geology of the Precambrian Palaeozoic rocks of northern Nigeria- review. In: C.A. Kogbe (Editor), Geology of Nigeria. Elizabethan Publishers and Co., Lagos, pp. 15-39.

McCurry, P. and Wright, J.B. (1977). Geochemistry of calc-alkaline volcanics in northwestern Nigeria and a possible Pan-African suture zone: *Earth Planetary Science Letter*, 37: 90-96.

Mwaniki., M. W., Moeller, M. S. and Schellmann. G. (2015). A comparison of Landsat 8 (OLI) and Landsat 7 (ETM+) in mapping geology and visualising lineaments: A case study of central region Kenya. The International Archives of the Photogrammetry, Remote Sensing and Spatial Information Sciences, Volume XL-7/W3, 2015 36th International Symposium on Remote Sensing of Environment, 11–15 May 2015, Berlin, Germany.

Obaje, N.G. (2009). Geology and mineral resources of Nigeria: *Springer Dordrecht Heidelberg London and New York, pp.* 221. http://dx.doi.org/10.1007/978-3-540-92685-6

Oversby, V.M. (1975). Lead isotope study of aplites from the Precambrian rocks near Ibadan, Southwestern Nigeria. *Earth Planetary Science Letters*, **27**, pp. 177-180.

Pour, A. B. and M. Hashim. (2012). "The application of ASTER remote sensing data to porphyry copper and epithermal gold deposits," Ore Geol. Rev., vol. 44, pp. 1–9.

Pournamdari, M., Hashim, M. and Beiranvand, A. (2014). "Spectral transformation of ASTER and Landsat TM bands for lithological mapping of Soghan ophiolite complex, south Iran," Adv. Sp. Res., vol. 54, no. 4, pp. 694–709.

Turner, D.C. (1983). Upper Proterozoic schist belts in the Nigerian sector of the Pan-African province of West Africa: *Precambrian Research*, 21: 55-79.

United States Geological Survey. (2013). Landsat 8: U.S. Geological Survey Fact Sheet 2013–3060, http://pubs.usgs.gov/fs/2013/3060/ (last date accessed: 25 November, 2014)

Woakes, M., Rahaman, M. A. and Ajibade, A. C. (1987). Some metallogenic features of the Nigerian Basement. *Journal of African Earth Sciences*, vol. 6, no. 5, pp. 655-664.

Wright, J.B., Hastings, D. A, Jones, W.B. and Williams, H. R. (1985). Geology and mineral resources of West Africa. *George Allen &Unwin, London*, ***187***, pp. 111-123.